Harlov, D. E. (2015): Fluids and Geochronometers: Charting and Dating Mass Transfer During Metasomatism and Metamorphism. - *Journal of the Indian Institute of Science*, *95*, 2.

http://journal.library.iisc.ernet.in/index.php/iisc/article/view/4552

Journal of the Indian Institute of Science
A Multidisciplinary Reviews Journal
ISSN: 0970-4140 Coden-JIISAD

REVIEWS

Fluids and Geochronometers: Charting and Dating Mass Transfer During Metasomatism and Metamorphism

Daniel Harlov[1,2]

Abstract | Many REE- and actinide-bearing minerals can act as both geochronological markers and recorders of geochemical processes. These include some of the most common REE- and actinide-bearing minerals found in igneous and mid- to high-grade metamorphic rocks such as monazite, xenotime, apatite, zircon, garnet, baddeleyite, huttonite, thorite, allanite, and titanite. The goal of this review is to describe the most recent research developments regarding these minerals, their interaction with each other, as well as their role as geochronometers.

Keywords: *geochronology, experimental petrology, apatite, monazite, xenotime, $ThSiO_4$, zircon, baddeleyite, garnet*

1 Introduction

In igneous and metamorphic rocks, REE- and actinide-bearing minerals can give both significant geochemical information (e.g. P-T-X constraints, fluid monitors, etc.), as well as geochronological information (e.g. crystallization age and/or the age of various metamorphic/metasomatic events), about a rock during its formation and subsequent geological evolution.

Extensively studied actinide- and REE-bearing minerals, such as zircon, garnet, fluorapatite, monazite, and xenotime, can be utilized to date multiple deformation and/or fluid-rock interaction events (e.g. Hoskin and Schaltegger, 2003; Davis et al., 2003; Williams et al., 2007; Hetherington et al., 2008; Thöni et al., 2008; Kohn, 2009; Chew and Spiking, 2015) through redistribution, addition, depletion, or substitution of REE, Th, U, Si, Na, and Ca via overgrowth, recrystallization, or pseudomorphic replacement in the form of coupled dissolution-reprecipitation processes (Putnis, 2002, 2009; Harlov et al., 2011). Temperature estimation of these events can be made via monazite-xenotime (Gratz and Heinrich, 1997, 1998; Heinrich et al., 1997; Andrehs and Heinrich, 1998), Ti-in-zircon (Watson et al., 2006), monazite-garnet (Pyle et al., 2001), and xenotime-garnet geothermometry (Pyle and Spear, 2000). Lastly, such events can give either general or more specific information on the chemistry and nature of the metasomatising fluids and/or melts responsible for the alteration or overgrowth (e.g., Harlov et al., 2005; Harlov and Dunkley, 2010; Harlov et al., 2011). The relationship between these minerals and other less utilized actinide- and (Y + REE)-bearing silicate minerals, such as zirconolite (e.g., Gieré et al., 1998), titanite (e.g., Harlov et al., 2006), and allanite (e.g., Finger et al., 1998; Wing et al., 2003; Budzyn et al., 2011), also allow for constraints to be placed on various actinide and (Y+REE) activities, oxygen and H_2O fugacities, and the subsequent chemical nature of fluids interacting with all of these minerals during episodes of fluid-rock interaction.

Understanding the chemical and physical relationship between these minerals as a function of P-T-X can add further insights into REE- and actinide-transport as a function of fluid/melt composition. With this in mind, the goal of this review is to make a general survey regarding our current understanding of REE- and actinide-bearing minerals and their geochemical and geochronological relationship with fluids.

2 Fluorapatite-Monazite-Xenotime

The occurrence of monazite [(Ce, LREE)(PO_4)] and/or xenotime [(Y, HREE)(PO_4)] as inclusions in fluorapatite [$Ca_5(PO_4)_3$(F, Cl, OH)] has been widely documented in high-grade metamorphic rocks (Fig. 1). The inclusions typically occur in granulite-

[1]*Deutches GeoForschungsZentrum, Telegrafenberg, D-14473 Potsdam, Germany.*
[2]*Department of Geology, University of Johannesburg, P.O. Box 524, Auckland Park, 2006 South Africa.*
dharlov@gfz-potsdam.de

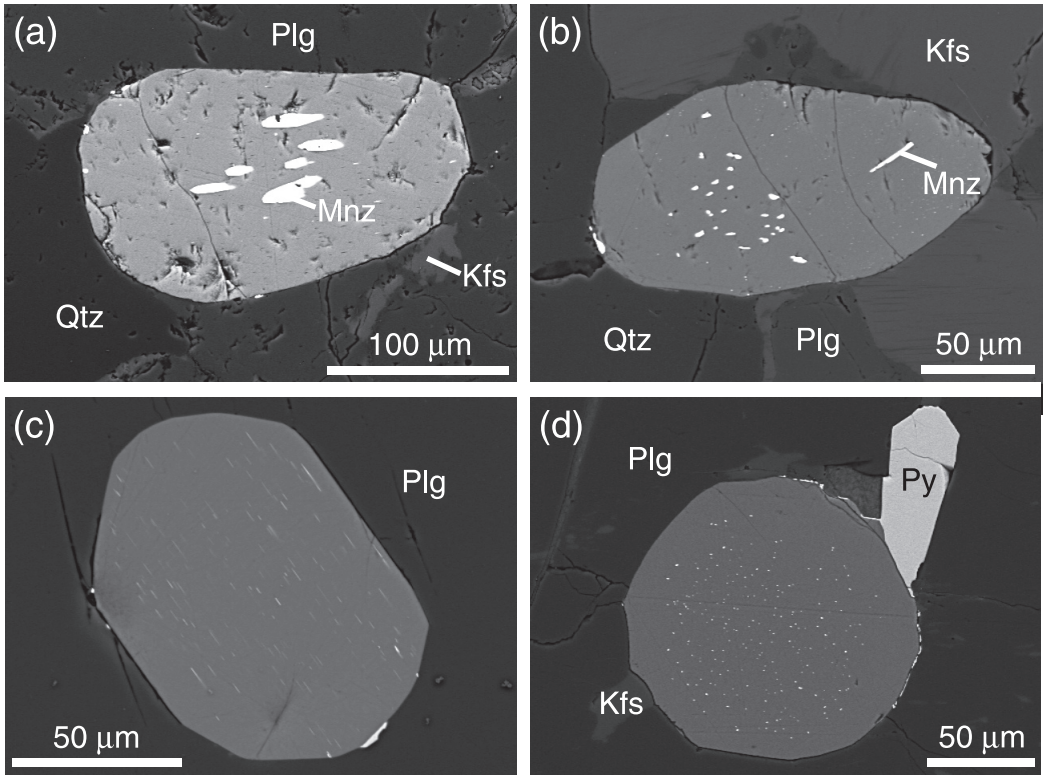

Figure 1: High-contrast back scattered electron (BSE) images of a variety of fluorapatite textures with metasomatically induced monazite (Mnz) inclusions and rim grains (bright) from a series of granulite-facies samples, the Shevaroy Block traverse, Tamil Nadu, S. India (Hansen and Harlov, 2007). (**a**) Fluorapatite grain with large-sized monazite inclusions partially elongated parallel to the c-axis. (**b**) Fluorapatite grain with moderately sized monazite inclusions; a fine powdering of very small (<1 μm) monazite inclusions is seen in some areas. In both Figs. 1a and 1b, some Ostwald ripening of the original small monazite inclusions has occurred, i.e. the larger monazite grains have consumed the smaller monazite grains and thus grown larger while the total number of inclusions is reduced. (**c**) Fluorapatite grain with numerous, very thin monazite inclusions epitaxially elongated with respect to the monazite b-axis parallel to the apatite c-axis. Monazite rim grain on lower right side. (**d**) Small monazite inclusions (<1 μm) in a fluorapatite grain cut perpendicular to the c-axis. Because the monazite grains are elongated parallel to the fluorapatite c-axis, as in Figure 1c, they appear as bright dots due to the cut of the fluorapatite crystal. Note the partial (bright) rim of secondary allanite. Plg—plagioclase, Kfs—K-feldspar, Qtz—quartz, Py—pyrite.

facies rocks as opposed to amphibolite-facies rocks where such inclusions tend to be absent (Harlov and Förster, 2002; Harlov et al., 2007a; Hansen and Harlov, 2007). Monazite and xenotime inclusions can also form in fluorapatite from fluid-rich granitic and mafic pegmatites (Harlov, 2011; Ziemann et al., 2005), in fluorapatite from Kiruna-type magnetite-apatite ore deposits directly after crystallization during cooling (Harlov et al., 2002a), in fluorapatite associated with gold deposits (Pan et al., 1993), as well as in chlorapatite from mafic layered intrusions and Cl-rich dykes associated with gabbros (Boudreau and McCallum 1990; Harlov et al., 2002b).

Inclusion formation has been directly linked to metasomatism by either external or internal H_2O-bearing fluids, though there is at least one exception to this general observation (Harlov et al., 2008). Here monazite, zircon, and minor xenotime were overgrown by fluorapatite during several cyclic episodes of crystallization in a granitic magma. Fluid-induced formation of monazite and xenotime inclusions in apatite is supported by experiments, which indicate that their formation and growth are the result of coupled dissolution-reprecipitation processes during metasomatic alteration (Putnis, 2002, 2009; Harlov et al., 2002b; Harlov and Förster, 2003; Harlov et al., 2005). Growth (or exsolution) of these inclusions by simple (Y+REE) diffusion in fluorapatite is highly unlikely due to their extremely slow diffusion rates (Cherniak et al., 2000).

During metasomatic alteration, Si and Na are removed from the apatite without the concurrent removal of (Y+REE). This results in a charge

imbalance, because (Y+REE) are stabilized in the apatite structure via the coupled substitutions (Pan and Fleet, 2002):

$$Si^{4+} + (Y + REE)^{3+} = P^{5+} + Ca^{2+} \quad (1)$$

and

$$Na^{+} + (Y + REE)^{3+} = 2Ca^{2+} \quad (2)$$

Removal of Na and Si, but not (Y+REE), allows for the fluid-aided nucleation and growth of monazite and/or xenotime either as inclusions in the apatite or as rim grains on the surface of the apatite. Once sufficient concentrations of REE have been reached in the fluid, nucleation and growth of monazite and/or xenotime inclusions in the apatite will occur via the following two general mass transfer reactions:

$$[Ca_{5-2x}, Na_x, REE_x]P_3O_{12}F + x\,[2\,Ca^{2+} + P^{5+}] \times (\text{from the fluid}) = Ca_5P_3O_{12}F + x\,REEPO_4 + x\,[Na^{+}] \times (\text{into the fluid}) \quad (3)$$

and

$$[Ca_{5-y}, REE_y][P_{3-y}, Si_y]O_{12}F + y\,[Ca^{2+} + 2\,P^{5+}] \times (\text{from the fluid}) = Ca_5P_3O_{12}F + y\,REEPO_4 + y\,[Si^{4+}] \times (\text{into the fluid}) \quad (4)$$

Formation of rim grains is most likely due to the fluid-aided diffusion of a portion of the (Y+REE) towards the apatite grain surface where it collects in sufficient concentrations so as to promote the nucleation and growth of monazite or xenotime. As a consequence, the composition of the monazite and/or xenotime normally reflects the (Y+REE+Th+U) abundances in the host apatite from which it is derived. This is seen in their generally low to negligible Th abundances (e.g., Harlov and Förster, 2002; Harlov et al., 2002a; Harlov et al., 2005; Hansen and Harlov, 2007), although there can be exceptions to this observation if the fluorapatite contains unusually high concentrations of Th, as in the case of the Durango fluorapatite (cf. Harlov and Förster, 2003). This particular case suggests high Th mobility in both H_2O and KCl brines under high-grade (900°C; 1000 MPa) conditions.

While commonly euhedral to subhedral in shape, a substantial minority of monazite and xenotime inclusions can also grow elongated along the b-axis with respect to the c-axis of the apatite in an epitaxial relationship (Fig. 1c; Pan et al., 1993). Euhedral to subhedral monazite inclusions have been demonstrated to grow in fluid-filled voids in small clumps of crystals (Figs. 2b and e; see discussion in Harlov et al., 2005).

Fluids found to induce formation of monazite and/or xenotime inclusions in apatite or as grains along apatite rims include H_2O, H_2O/CO_2 fluids, and KCl+H_2O (Harlov et al., 2002b; Harlov and Förster, 2003) as well as 1 N H_2SO_4, and 1 N HCl (Fig. 2a; Harlov et al., 2005). Monazite and xenotime inclusions and rim grains can also form in fluorapatite from metapelites, which have experienced partial melting during granulite-facies metamorphism (Harlov et al., 2007a). In such cases, the fluorapatite can also experience partial dissolution presumably releasing (Y+REE) into the H_2O-alkali-SiO_2-rich melt. Other fluids, such as $CaCl_2$+H_2O or NaCl+H_2O, inhibit the growth of these inclusions and rim grains due to the ability of Ca and Na to enter the apatite structure and charge balance or replace the (Y+REE). Exceptions to this rule are seen in solubility experiments involving a REE-bearing fluorapatite in NaCl brines at 700–900°C and 700–2000 MPa (Antignano and Manning, 2008). Here small crystals of monazite formed on the surface of the fluorapatite during its partial, incongruent dissolution in the brine. This behaviour is also seen in the incongruent dissolution of (Y+REE)-bearing fluorapatite in peraluminous granitic melts (Wolf and London, 1995).

Regions of the apatite affected by coupled dissolution-reprecipitation are characterized by a pervasive, inter-connected micro- and nano-porosity, which allows for fluids to infiltrate (Figs. 2b, c, d; Harlov et al., 2005). The presence of an interconnected fluid medium greatly speeds up mass transfer allowing for the rapid (hours–days) growth of monazite and/or xenotime inclusions by utilizing the available P, Y, and REE, while the micro- and nano-pores provide random nucleation sites (Figs. 2b and e). Monazite and xenotime inclusions, as well as rim grains, can form over a wide P-T range, i.e. 100–1000 MPa and 100–900°C (see review in Harlov et al., 2002b; Harlov et al., 2005). Consequently, whether or not nucleation will occur is highly dependent on the level of reactivity between the fluid and the apatite (cf. Harlov et al., 2002b; Harlov and Förster, 2003; Harlov et al., 2005).

In corroboration with what has already been concluded from nature (e.g., Harlov and Förster, 2002; Harlov et al., 2002a,b; Hansen and Harlov, 2007) and experimentally (Harlov et al., 2002b; Harlov and Förster, 2003; Harlov et al., 2005), monazite and xenotime associated with fluorapatite can serve as a valuable "fingerprint" for recording metasomatic events in high-grade metamorphic rocks. The presence of co-existing monazite and

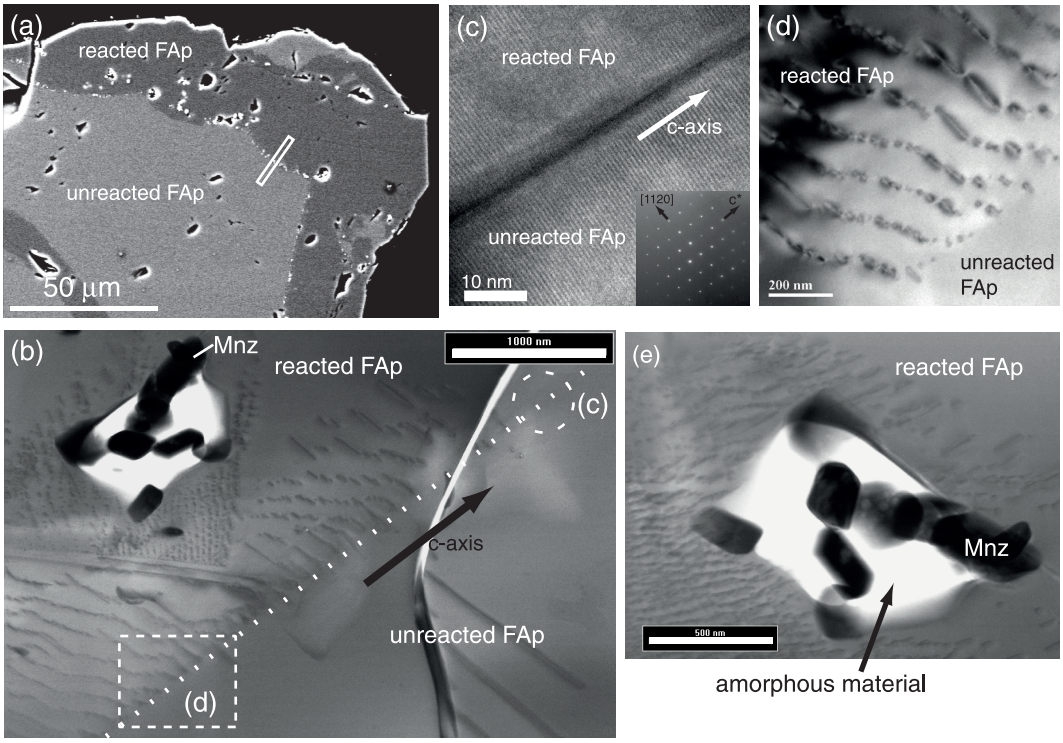

Figure 2: (**a**) High-contrast back scattered electron (BSE) photographs of fluorapatite reacted with 1 N HCl at 600°C and 500 MPa for 3 weeks (Harlov et al., 2005). Dark regions have reacted with the HCl solution and are depleted in REE + Si + Na + S + Cl. Bright areas represent unreacted apatite. Numerous, bright, small monazite inclusions outline the reaction front between the reacted and unreacted regions. Fig. 2b is a transmission electron microscopy (TEM) foil cut across the reaction front, which is denoted by the dotted line. The location of the TEM foil is designated by the elongated rectangle in Fig. 2a. The arrow indicates the approximate direction of the fluorapatite c-axis. The reacted fluorapatite consists of a series of sub-parallel nano-channels and group of monazite grains in a cavity filled with an amorphous quenched material enriched in Cl and REE relative to the surrounding fluorapatite. Fig. 2c shows a high resolution TEM lattice fringe image of the interface between the reacted and the unreacted fluorapatite taken from the region within the dashed circle. Note that the lattice fringes are continuous across the interface indicating that the pattern of the crystallographic lattice from the unreacted fluorapatite has been transmitted to the reacted fluorapatite. A close-up of the nano-channels is shown in Fig. 2d. Fig. 2e shows a close-up of the void, and a cluster of randomly oriented euhedral monazite grains. The void is surrounded by an array of nano-channels. FAp—fluorapatite, Mnz—monazite.

xenotime inclusions in fluorapatite, as well as rim grains, can give some indication of the temperature of the metasomatic overprint via monazite-xenotime geothermometry (cf. Gratz and Heinrich, 1997, 1998; Heinrich et al., 1997; Andrehs and Heinrich, 1998). In such cases, co-existing monazite and xenotime inclusions tend to give higher temperatures as opposed to rim grains (e.g., Harlov and Förster, 2002). More importantly, the association of monazite and/or xenotime with fluorapatite or chlorapatite helps to place constraints on the chemistry of the infiltrating fluids responsible for the metasomatism of the apatite as well as the rock as a whole. In this respect, fluorapatite from high-grade rocks, that contain monazite and/or xenotime inclusions/rim grains, potentially represents a record of metasomatic events over a wide range of temperatures and specific fluid compositions in addition to serving as a major host for LREE. Lastly, the metasomatic event(s) can be timed using monazite/xenotime U-Pb geochronology (cf. Williams et al., 2007) and/or apatite U-Pb, (U-Th)/He, and Lu-Hf thermochronology (Chew and Spikings, 2015). In the latter case, since metasomatised areas in the apatite are chemically altered such that U, Th, and Lu are either added, removed, or reduced, and assuming that decay products such as Pb and He are totally removed, these areas could potentially be used to date the metasomatic event responsible for their generation relative to the original unaltered apatite.

3 Monazite-Xenotime-$ThSiO_4$

In metamorphic rocks, monazite and xenotime may either grow as the net product of a series of mineral reactions or be inherited from igneous

and/or sedimentary precursors. In igneous rocks, typically peraluminous granites and granitoids, monazite and xenotime tend to be among the first minerals to crystallize out of the melt (Bea, 1996). In either case, any Th in the system will be strongly partitioned into monoclinic monazite as the monoclinic huttonite [$ThSiO_4$] and/or monoclinic cheralite [$CaTh(PO_4)_2$] component via the coupled substitution reactions:

$$Th^{4+} + Si^{4+} = REE^{3+} + P^{5+} \quad (5)$$

and

$$Th^{4+} + Ca^{2+} = 2REE^{3+}, \quad (6)$$

respectively (Förster, 1998; Zhu and O'Nions, 1999; Seydoux-Guillaume et al., 2002a). To a lesser extent, Th will also partition into xenotime as the tetragonal thorite [$ThSiO_4$] component via coupled substitution reaction (5) (Hetherington and Harlov, 2008; Harlov and Wirth, 2012). Uranium can be incorporated into either monazite or xenotime as the tetragonal coffinite [$USiO_4$] component:

$$U^{4+} + Si^{4+} = REE^{3+} + P^{5+}, \quad (7)$$

though tetragonal xenotime commonly takes in more U relative to co-existing monoclinic monazite. (Seydoux-Guillaume et al., 2002b; Kositcin et al., 2003; Krenn et al., 2008). Experimentally, it has been demonstrated that monazite may be partially overgrown or partially replaced by pure monoclinic huttonite via coupled dissolution-reprecipitation, suggesting that $ThSiO_4$ grains associated with partially altered monazite in nature are actually huttonite as opposed to lower grade tetragonal thorite (Harlov et al., 2007b).

Fluid-aided alteration of Th- and U-bearing xenotime and monazite megacrysts in a granitic pegmatite (Hidra, SW Norway) resulted in the formation of thorite and uraninite [UO_2] inclusions in the altered areas in a manner similar to that seen for the formation of monazite and xenotime inclusions in apatite (Hetherington and Harlov, 2008). The mechanism behind the formation of these inclusions is similar, invoking a fluid-filled, pervasive porosity resulting from coupled dissolution-reprecipitation and the subsequent nucleation of thorite and uraninite inclusions in a random sampling of these pores (cf. Putnis, 2002, 2009).

The current role of monazite and xenotime in dating from one to multiple events during metamorphism and/or deformation either singly (e.g. Pyle and Spear, 2003; Pyle et al., 2005; Mahan et al., 2006 a,b; Williams et al., 2007; Dumond et al., 2008; Hetherington et al., 2008), or in conjunction with allanite (Janots et al., 2009) or fluorapatite (Finger and Krenn, 2007) has increased the geochronological versatility of either mineral. This, coupled with the concurrent utilization of both minerals in geothermometry (Gratz and Heinrich, 1997, 1998; Heinrich et al., 1997; Andrehs and Heinrich, 1998; Pyle and Spear, 2000; Pyle et al., 2001), as well as tracking their metasomatic derivation from apatite as inclusions and rim grains (Harlov et al., 2005), have greatly increased the amount of information that can be extracted from these two common accessory minerals.

Once formed, metamorphic monazite or xenotime can be partially or totally altered with respect to the Th, U, and (Y+REE) distribution and content (Fig. 3). Though such alteration with respect to Th is not as common in metamorphic xenotime, since it incorporates considerably less Th than co-existing monazite in the same rock (e.g., Franz et al., 1996). During alteration, Th can either be gained or lost by monazite or xenotime in variable amounts such that a pattern of patchy, curvilinear intergrowths with sharp compositional boundaries, either depleted or enriched in $ThSiO_4$-$CaTh(PO_4)_2$, develop in the body of the original monazite grain (Fig. 3).

The conclusion reached by most studies of Th-depleted or -enriched textures in monazite hypothesizes that this alteration is a metasomatically induced process due to the presence of locally mobile Th, Si, Ca, P, and (Y+REE) in a grain boundary/pore fluid that is reactive with respect to the monazite or xenotime (e.g., Bingen and van Breemen, 1998). This is supported by the extremely slow diffusion rates in monazite for both Th, due to its coupled substitution with Si and Ca via reactions (5) and (6) (Cherniak and Pyle, 2008), and Pb (Cherniak et al., 2004). However, speculations on the exact nature of this fluid are more vague. In general, these intergrowths tend to give different, and generally younger, electron microprobe ages compared to areas of the monazite grain unaffected by metasomatic alteration (Poitrasson et al., 1996; Seydoux-Guillaume et al., 2003; Goncalves et al., 2005; Williams et al., 2006, 2007, 2011; Dumond et al., 2008).

In order to determine whether or not metasomatic alteration could be responsible for these textures, a series of metasomatism experiments were performed at granulite-facies temperatures

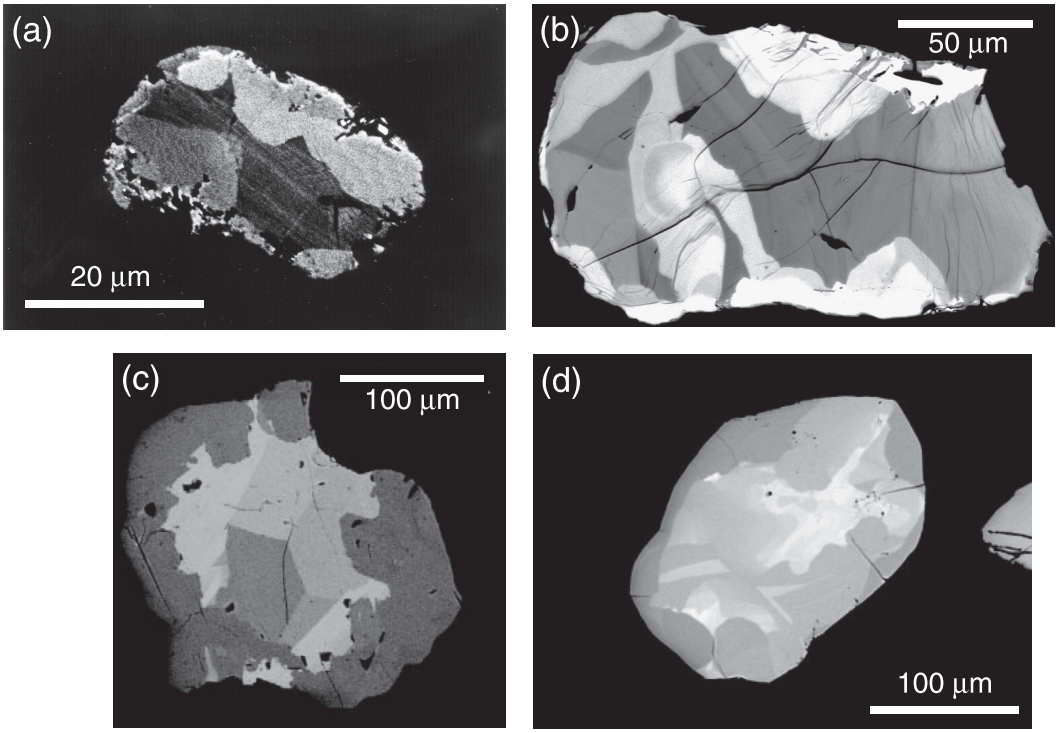

Figure 3: Examples from nature of partially metasomatised monazite in both metamorphic and granitoid rocks, which have experienced either Th gain or loss (high contrast back scattered electron (BSE) imaging). (**a**) Partially metasomatised monazite, with Th-enriched embayments, from a granulite-facies metabasite, Val Strona high-grade traverse, Ivrea-Verbano Zone, Northern Italy (Förster and Harlov, 1999). Some Th-enriched regions contain up to 30% of the huttonite component. The metabasites have been metasomatised by fluids both from intercalated metapelite layers as well as from emplacement of the Mafic Formation at the base of the traverse. (**b**) Partially metasomatised monazite in clinopyroxene-bearing amphibolite-facies and orthopyroxene-bearing granulite-facies orthogneisses, Rogaland-West Agder terrain, SW Norway (Bingen and van Breemen, 1998). The surrounding pore fluids are ascribed to being responsible for the formation of both Th-enriched and Th-depleted embayments along the monazite grain rim. (**c**) Partially metasomatised monazite grain, with both Th-enriched and Th-depleted rims, from the peraluminous, two mica St Laurent granite intruding local migmatites, granites, and mica schists, Massif Central, France (Cocherie et al., 2005). (**d**) Partially metasomatised monazite grain from a sheet of Paleoproterozoic garnet bearing monzogranite from the Trans-Hudson Orogen, Baffin Island, Canada (St Onge et al., 2007).

and pressures (900°C, 1000 MPa) in the piston cylinder apparatus (CaF_2 assembly; cylindrical graphite over) for 2–25 days and at amphibolite-facies temperatures and pressures (600°C, 500 MPa) for 23–49 days using cold-seal autoclaves on a hydrothermal line (Fig. 4; Hetherington et al., 2010; Harlov and Hetherington, 2010; Harlov et al., 2011). The experiments utilized fragments (10–200 μm) from natural, inclusion-free, euhedral monazite (500–1500 μm) grains from a heavy mineral, beach sand (North Carolina, USA), which is relatively homogeneous with respect to Th (7–8 ThO_2 wt%), plus a variety of high pH, alkali-bearing fluids, i.e. 2N NaOH, 2N KOH, and $Na_2Si_2O_5$ + H_2O, sealed into Au capsules. The source of Si in these experiments was quartz or $Na_2Si_2O_5$, whereas the source of Th is presumed to have resulted from the total dissolution of the smallest monazite grain fragments into the fluid. There is no evidence for the leaching of Th from the monazite grain fragments because unmetasomatised areas of the monazite have the same composition as the original monazite. These fluid compositions were chosen as the ones that might possibly exist along grain boundaries in a feldspar-bearing rock infiltrated by H_2O-bearing fluids (e.g. alkali-bearing brines or H_2O-CO_2) under a variety of metamorphic conditions ranging from low- to high-grade.

In each experiment, the monazite reacted with the fluid such that limited metasomatised regions of variable enrichment in the huttonite component occurred, resulting in textures similar to that seen in nature (Fig. 4; Harlov and Hetherington, 2010; Harlov et al., 2011). The metasomatised regions are separated from the non-metasomatised regions by sharp, curvilinear

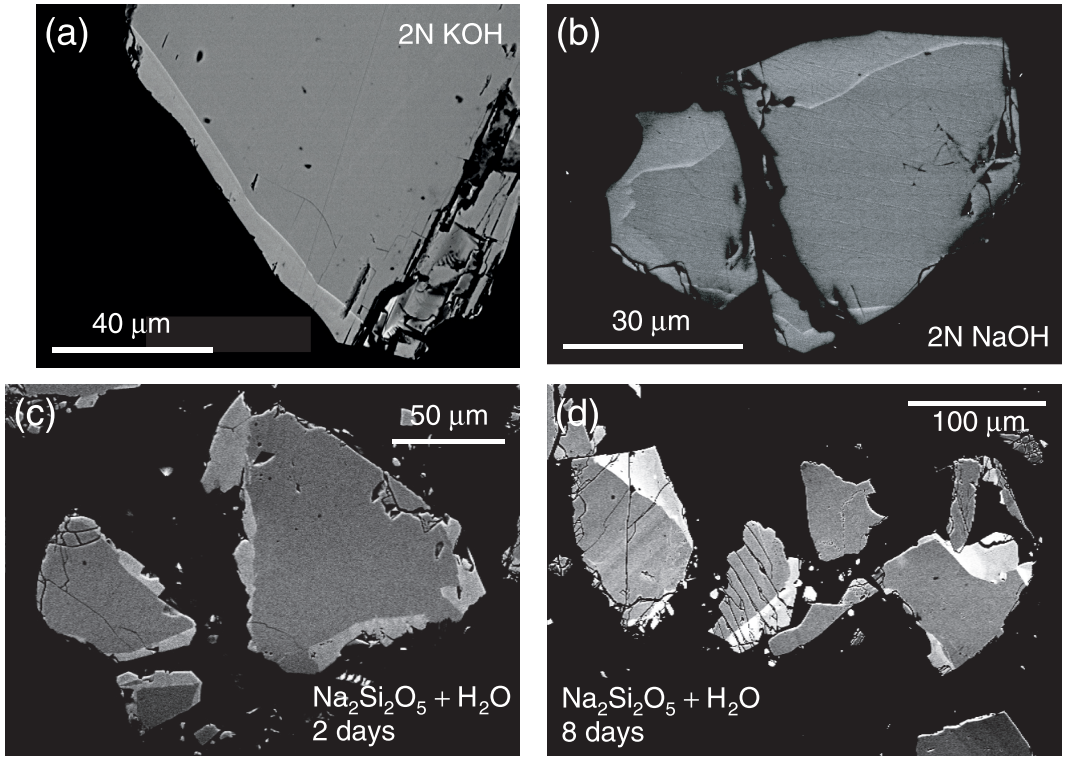

Figure 4: High contrast back scattered electron (BSE) images of monazite grains experimentally metasomatised in alkali-bearing fluids at 900°C and 1000 MPa using a CaF_2 assembly in the piston cylinder press (Harlov et al., 2011). Bright, altered areas are enriched in Th + Si + Ca relative to the dark areas (original monazite). Any cracks seen occurred during the mounting and polishing process of the monazite grain fragments. (**a**) Monazite grain metasomatised in a 2N KOH solution for 8 days. (**b**) Monazite grain metasomatised in a 2N NaOH solution for 25 days. (**c**) Monazite grain metasomatised in a $Na_2Si_2O_5 + H_2O$ solution for 2 days. (**d**) Monazite grain metasomatised in a $Na_2Si_2O_5 + H_2O$ solution for 8 days.

or straight compositional boundaries. Some metasomatised regions also show peculiar enrichments in the huttonite component that appear to be crystallographically controlled. In a manner similar to that seen in the apatite metasomatism experiments, the alkali-bearing fluid appears to have attacked the monazite grains in a coupled process through the partial dissolution of the pre-existing monazite followed concurrently by the reprecipitation of new monazite enriched in the $ThSiO_4$ component. This resulted in the pseudomorphic, partial replacement of the original monazite. It also presumes that Th and Si quickly reached saturation or possible super-saturation in the fluid, followed by strong partitioning into the reprecipitated monazite during this coupled dissolution-reprecipitation process (Putnis, 2002, 2009; see discussion in Harlov et al., 2011). Dating these intergrowths can also potentially date the metasomatic event responsible for them (Williams et al., 2011). This presumes that all the Pb has been removed during metasomatic alteration, which is the case when $Na_2Si_2O_5 + H_2O$ is the metasomatising fluid (see Harlov et al., 2011; Williams et al., 2011).

In a series of similar metasomatism experiments, fragments (10–200 μm) of a natural, inclusion-free, euhedral, Th-absent xenotime (pegmatite, Northwest Frontier Province, Pakistan), was enriched in specific areas with respect to Th+Si utilizing a series of alkali-bearing fluids that include 2N NaOH, 2N KOH, $Na_2Si_2O_5+H_2O$, and $NaF+H_2O$, in addition to ThO_2 and SiO_2 (Fig. 5; Harlov and Wirth, 2012). Charge and fluid were sealed in Au capsules and placed in the piston-cylinder apparatus (CaF_2 assembly; cylindrical graphite over) at 1000 MPa and 900°C (8–25 days) or cold seal autoclaves on a hydrothermal line at 500 MPa and 600°C (23 days). BSE imaging, electron microprobe analysis, and transmission electron microscopy (TEM) indicate that a fraction of the xenotime grains in the 2N KOH, $Na_2Si_2O_5+H_2O$, and $NaF+H_2O$ experiments have altered areas enriched in Th+Si. No reaction was observed in the 2N NaOH experiments. The altered areas occur as a series of curvilinear intergrowths with sharp compositional

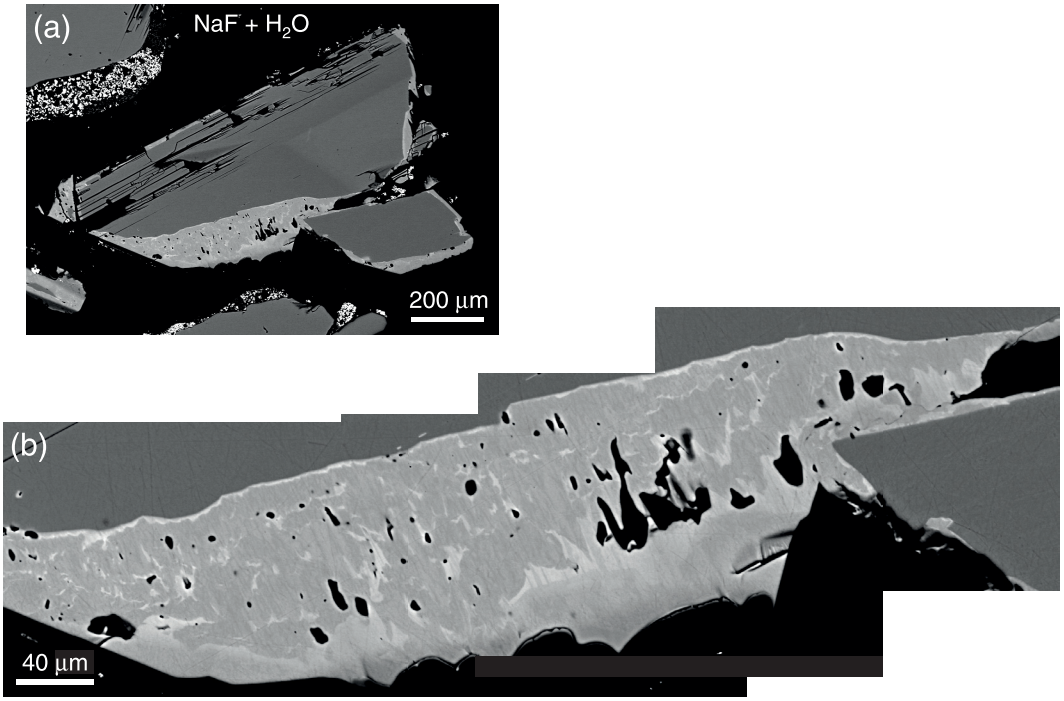

Figure 5: (**a**) High contrast back scattered electron (BSE) image of xenotime grain metasomatised in ThO_2 + SiO_2 + NaF + H_2O at 900°C and 1000 MPa for 8 days (Harlov and Wirth, 2012). Bright, altered areas are enriched in Th+Si relative to the dark areas (unaltered xenotime). (**b**) Close-up showing the extensive microporosity in metasomatised areas of the xenotime. Note the uneven distribution of Th+Si in the altered area.

boundaries that extend from the edge of the xenotime grain into the interior. Similar to what has been described for monazite, the formation of these Th+Si enriched areas are interpreted to be a consequence of fluid-mediated coupled dissolution-reprecipitation (Putnis, 2002, 2009; Harlov et al., 2011; Harlov and Wirth, 2012). One important implication from these experiments is that the altered Th-enriched areas in the xenotime could be reset geochronologically similar to what is observed for monazite (Williams et al., 2011), allowing for the metasomatic event to be dated. This assumes that all the Pb has been removed from the altered areas during their genesis.

In a comparable study, specific areas of the same natural Th-absent, low U xenotime have been experimentally enriched in U+Si utilizing a NaF+H_2O fluid plus UO_2 and SiO_2 under both reducing (graphite-CO/CO_2 buffer) and oxidizing (Mt-Hm buffer) conditions (Fig. 6; Harlov, work in progress). Charge and fluid were sealed in 2 cm long, 3 mm diameter Au and Pt capsules. In the reduced experiment, the Au capsule was placed in the piston-cylinder apparatus (CaF_2 assembly; graphite oven; 1000 MPa; 900°C; 8 days). In the oxidized experiment (500 MPa; 900°C; 4 days) the Pt capsule was packed with Hm+H_2O into a 4 cm long, 5 mm diameter Pt capsule, which was placed in the internally heated gas pressure vessel. BSE imaging indicates that the altered areas occur as a series of curvilinear intergrowths with sharp compositional boundaries that extend from the edge of the xenotime grain into the interior. Electron microprobe analysis indicates that the altered areas from both experiments are enriched in U+Si via coupled substitution reaction (7). WDS element distribution maps indicate that U+Si are concentrated close to the sharp compositional interface between the altered and unaltered xenotime with corresponding depletion in Y+HREE while showing a more uniform enrichment across the rest of the altered area (Fig. 6b). Across the altered region Y occurs as a series of concentric waves of relative enrichment and depletion with contrasting depletion and enrichment in HREE. Element movement is interpreted as a consequence of fluid-mediated, coupled dissolution-reprecipitation (Putnis, 2002, 2009) in some sort of a chromatographic column effect across the altered area. Fluid-aided incorporation or depletion of U into xenotime has implications with respect to its utilization as a metamorphic geochronometer, assuming that all the original Pb in the altered areas has been removed, thus resetting the U-Th-Pb xenotime geochronometer.

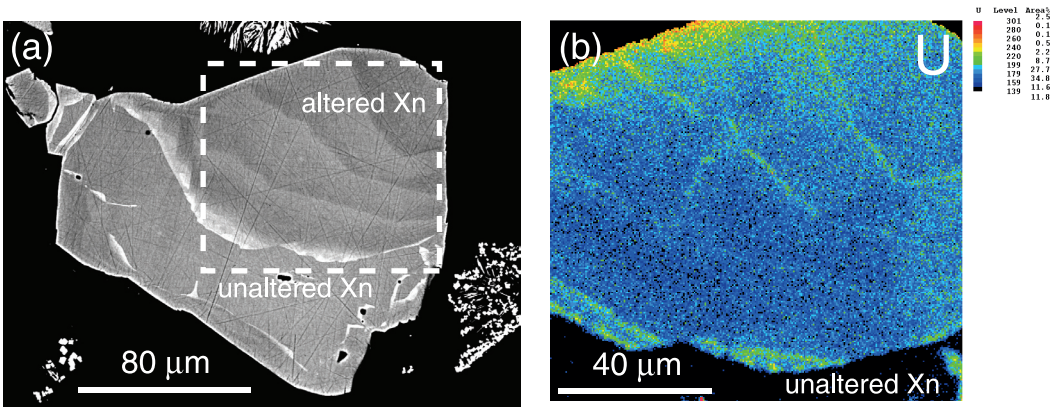

Figure 6: (**a**) High contrast back scattered electron (BSE) image of xenotime grain metasomatised in UO_2+SiO_2+NaF+H_2O buffered to magnetite-hematite oxygen fugacity at 900°C and 500 MPa for 4 days (Harlov, 2015, work in progress). (**b**) Uranium element map of the metasomatised area outlined by the dashed box in (**a**). The metasomatised area is enriched in U+Si, and hence lighter under BSE imaging compared to the darker, original, unmetasomatised xenotime.

4 Zircon

The role of zircon [$ZrSiO_4$] in high-grade metamorphic rocks is primarily that of a U-Th-Pb geochronometer (see review by Davis et al., 2003), though it does contain significant trace amounts of Ti, HREE, and Y in addition to Th, U, and Hf (Hoskin and Schaltegger, 2003). These trace elements can show relative enrichment or depletion in zircon depending on the geochemical environment of the rock (e.g., Cherniak and Watson, 2003; Schulz et al., 2006; Harley and Kelly, 2007; Kebede et al., 2007; Wu et al., 2008) or, as in the case of Ti, act as a geothermometer in the presence of co-existing rutile in both metamorphic and igneous rocks (Watson et al., 2006; Ferry and Watson, 2007; Cherniak and Watson, 2007; Bin et al., 2008; Hiess et al., 2008; Ferriss et al., 2008). Zircon can also be metasomatically altered via coupled dissolution-reprecipitation processes with respect to trace element compositions (Fig. 7a; Geisler et al., 2007; Rubatto et al., 2009).

The stability of zircon, in the presence of various possible metamorphic and igneous fluids under a range of P-T conditions and its subsequent alteration with respect to some of these fluids, has begun to be explored as well as speculated upon in a series of experimental studies of metasomatised zircons by Geisler et al., (2007). These experiments indicate that alteration of zircon takes place either via dissolution coupled with overgrowth or else via fluid-aided coupled dissolution-reprecipitation (Putnis, 2002, 2009). This process results in the zircon being partially or totally replaced by either new, compositionally re-equilibrated zircon or a new mineral phase.

In a study by Harlov and Dunkley (2010), (see also Harlov et al. work in progress), fragments (50 to 200 microns) from a large, inclusion-free, clear, light brown, relatively non-metamict euhedral zircon collected from a nepheline syenite pegmatite (Seiland magmatic province, northern Norway) were experimentally reacted in 20 mg batches with a series of alkali-and Ca-bearing fluids plus a Th+Si source (5 mg ThO_2 + $ThSiO_4$ + SiO_2) in sealed Pt capsules at 900°C and 1000 MPa for 6 to 11 days in the piston cylinder press using a CaF_2 setup with cylindrical graphite oven. Fluids included 5 mg 2N NaOH, 5 mg 2N KOH, 10 mg $Na_2Si_2O_5$ + 5 mg H_2O, 1 mg NaF + 5 mg H_2O, and 1–5 mg $Ca(OH)_2$ + 5 mg H_2O. In each experiment, the zircon grain fragments reacted with the fluid. This reaction took the form of partial replacement of the zircon with compositionally altered zircon via coupled dissolution-reprecipitation plus varying amounts of overgrowth (Figs. 7b, c). The reacted zircon is characterized by a sharp compositional boundary between the altered and original zircon, as well as in some cases, by a micro-porosity and/or inclusions of ZrO_2 or $ThSiO_4$. Sensitive high resolution ion microscopy (SHRIMP) and laser ablation inductively coupled plasma mass spectrometry (LA-ICPMS) analysis of altered areas in the zircon indicates that it is strongly enriched in Th+Si, heavily depleted in U, and heavily to moderately depleted in (Y+REE). If YPO_4 replaces (Th+Si) in the system, the altered zircon is enriched in YPO_4 and heavily depleted in Th and U. In all the experiments, radiogenic ^{206}Pb (3 to 5 ppm

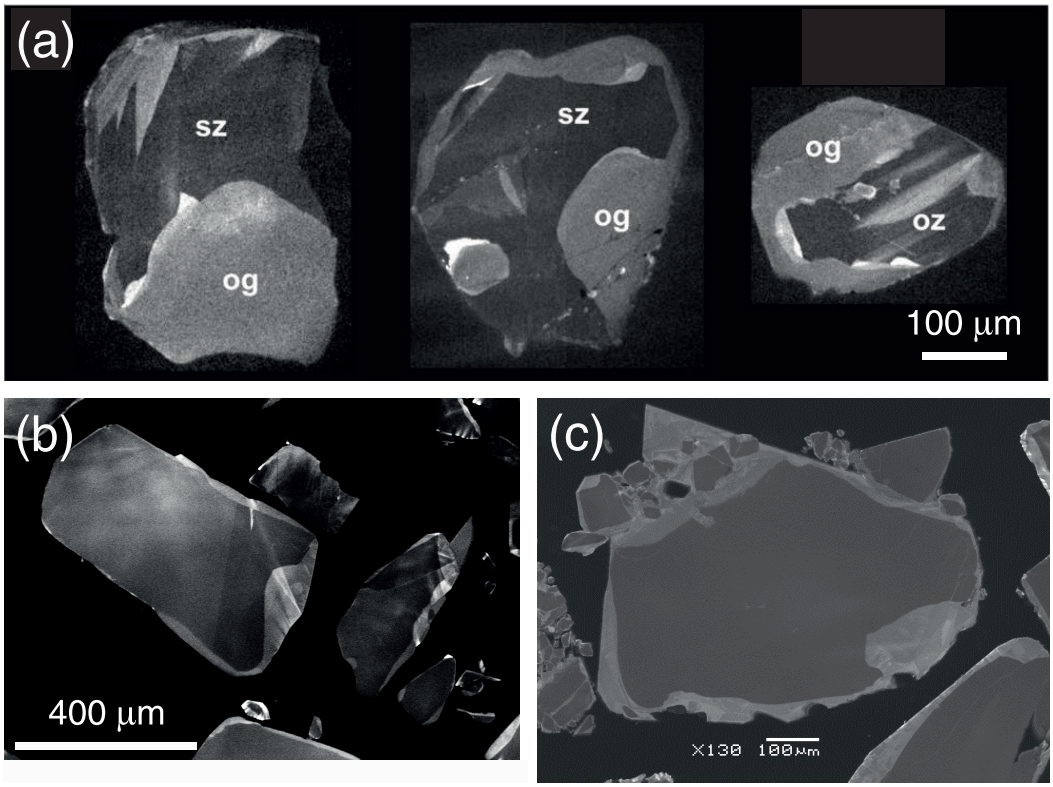

Figure 7: (**a**) Cathodoluminescence (CL) images of partially altered zircons from a 983 Ma anorthosite, Eastern Ghats Belt, India (Chatterjee et al., 2008). Sector zoned—sz; overgrowth—og; oscillatory zoned—oz. The sz and oz areas are unaltered zircon, whereas the og areas are altered zircon depleted in U relative to the darker areas. (**b**) and (**c**) CL images of natural Seiland zircon metasomatised in $ThO_2+SiO_2+NaF+H_2O$ at 900°C and 1000 MPa for 6 days (Harlov et al., 2015, work in progress). Bright altered areas are enriched in Th and depleted in U and REE and totally depleted in Pb relative to the darker unaltered zircon.

in the unaltered zircon) is strongly depleted in the altered zircon, such that it is below SIMS detection limits. Hafnium concentrations in the altered zircon show either some minor depletion or retain the same value as in the original zircon. The results from these experiments indicate that zircon can be compositionally altered via alkali- and Ca- bearing fluids via coupled dissolution-reprecipitation processes (Putnis, 2002, 2009) under high-grade conditions and that their internal geochronometer can be reset due to the complete loss of radiogenic Pb. Regarding the relative complexity of natural zircons in both igneous and metamorphic rocks as well as detrital zircons in sedimentary rocks, the results from these experiments have important implications in sorting out zircon textures with regard to what they can tell us regarding both the protolith, in which the zircon formed as well as the subsequent metamorphic/metasomatic events to which the zircon was later subjected to. This information takes the form of geochronological and geochemical data potentially allowing for metamorphic/metasomatic events to be dated, while giving additional information regarding the nature and chemistry of the fluids present.

5 Zircon-Baddeleyite

Like zircon, baddeleyite [ZrO_2] is commonly utilised for U-Th-Pb geochronology. Unlike zircon, baddeleyite can only form under silica under-saturated conditions. Examples where baddeleyite has been replaced by zircon due to increasing silica saturation during metamorphism are common, though examples of the reverse reaction are relatively rare.

Naturally occurring intergrowths of baddeleyite have been found to occur in a scattering of zircon grains from albitised areas in quartz-bearing felsic metamorphic rocks (granitoid gneisses, schists, and quartzite) from Greenland and Ghana (Lewerentz et al., work in progress). Baddeleyite occurs either as bands concordant with zircon

growth zoning, or as blobs randomly distributed within the grain. The intergrowths are commonly accompanied by altered zircon zones, which contain non-stoichiometric elements such as Na, Al, Ca, and Fe.

In order to understand why baddelyite would form in zircon from quartz-saturated rocks, Lewerentz et al. (work in progress) conducted a series of experiments using natural zircon grains, SiO_2, H_2O, and $CaCl_2$ or $Ca(OH)_2$ (CaF_2 setup, cylindrical graphite oven, piston cylinder press; cold seal autoclave, hydrothermal line). Conditions were 500–1000 MPa, 600–900°C, and 4–50 days. Experimental results indicate that zircon partially altered to baddeleyite if the molar amount of Ca was greater than the molar amount of Si in the system. In contrast, if Si > Ca the zircon remained pristine, and no baddeleyite formed. Scanning electron microscopy and electron microprobe analysis evaluation of the reacted grains shows that baddeleyite primarily takes the form of bead-like trails along the reaction front. Ca-silicate-filled pores form in the rim. SIMS evaluation shows that Th, U, Pb, and Y+REE have been mobilised. Uranium is detected in both the new-formed baddeleyite and altered zircon rims, whereas Pb is below the SHRIMP detection limit.

Formation of baddeleyite from zircon in silica-saturated rocks appears to be only possible when Ca saturates the system such that the Si is tied up as $CaSiO_4$ lowering the silica activity to below 1. This allows baddeleyite to form only on a highly localized grain boundary scale in areas where the Si activity has been lowered below one due to excess Ca in the local system despite the general presence of quartz in the rock overall. Total Pb loss during alteration in both the reacted areas of the zircon and in the newly formed baddeleyite allows for either to be used to date the metasomatic event responsible for their formation.

6 Conclusions and Future Work

It is obvious from this brief review that a number of the more commonly used phosphate and silicate geochronometers can be partially, if not totally, altered by fluids that reasonably can be expected to exist in igneous and metamorphic rocks in the Earth's crust. In addition to several common acids (HCl and H_2SO_4), these fluids are principally alkali-bearing brines and bases whose existence is practically guaranteed when H_2O encounters the Na-K-Ca feldspar-rich rocks of the Earth's crust. The fact that, partially, if not totally, altered geochronological minerals such as apatite (Figs. 1,2), monazite (Figs. 3,4), xenotime (Figs. 5, 6), or zircon (Fig. 7) are commonly encountered in nature, and that experiments, involving acids and alkali-bearing fluids, have replicated these textures, provides strong evidence that similar fluids in nature could also be responsible for the alteration of these minerals and the potential resetting of their geochronological clocks during igneous and metamorphic processes.

Future work regarding these minerals essentially represents the continuation of an approach consisting of experimental replication, once certain hypotheses have been formulated from natural observation. In addition to continuing experimental work on apatite, monazite, xenotime, and zircon, as outlined in this review, new experiments need to be formulated for titanite, allanite, and zirconolite, which are barely covered here. Lastly, natural observation and experimental replication need to be confirmed by thermodynamic verification, which, in essence, completes the circle of inquiry. While some attempts have been made in this direction (e.g., Spear, 2010), little additional progress has been made due, in part, to a lack of good thermodynamic data on these minerals. This only re-emphasizes the need for additional, well thought-out experiments, coupled with natural observation, before this system can be properly geochemically modelled with an emphasis on these minerals as geochronometers that can be affected and reset by fluids.

Acknowledgements

This review has benefited from numerous collaborations and discussions with various colleagues over the years regarding the minerals mentioned here. In addition, collaborations and discussions with various colleagues over the years and technical support, under the direction of Wilhelm Heinrich, at the GeoForschungsZentrum have all contributed to this article.

Received 21 February 2015.

References

G. Andrehs and W. Heinrich, Experimental determination of REE distributions between monazite and xenotime: Potential for temperature-calibrated geochronology, *Chemical Geology*, **149**, 83 (1998).

A. Antignano and C. E. Manning, Fluorapatite solubility in H_2O and H_2O-NaCl at 700 to 900 °C and 0.7–2.0 GPa, *Chemical Geology*, **251**, 112 (2008).

F. Bea, Residence of REE, Y, Th and U in granites and crustal protoliths: Implications for the chemistry of crustal melts, *Journal of Petrology*, **37**, 521 (1996).

F. Bin, F. Z. Page, A. J. Cavosie, J. Fournelle, N. T. Kita, J. S. Lackey, S. A. Wilde and J. W. Valley, Ti-in-zircon thermometry: applications and limitations, *Contributions to Mineralogy and Petrology*, **156**, 197 (2008).

B. Bingen and O. van Breemen, U-Pb monazite ages in amphibolite- to granulite-facies orthogneiss reflect hydrous mineral breakdown reactions: Sveconorwegian Province of SW Norway, *Contributions to Mineralogy and Petrology*, **132**, 336 (1998).

B. Budzyn, D. E. Harlov, M. L. Williams and M. J. Jercinovic, Experimental determination of stability relations between monazite, fluorapatite, allanite, and REE-epidote as a function of pressure, temperature, and fluid composition, *American Mineralogist*, **96**, 1547 (2011).

A. E. Boudreau and I. S. McCallum, Low-temperature alteration of REE-rich chlorapatite from the Stillwater Complex, Montana, *American Mineralogist*, **75**, 687 (1990).

N. Chatterjee, J. Crowley, A. Mukherjee and S. Das, Geochronology of the 983-Ma Chilka Lake anorthosite, Eastern Ghats Belt, India: Implications for Pre-Gondwana tectonics, *Journal of Geology*, **116**, 105 (2008).

D. J. Cherniak, Rare earth element diffusion in apatite, *Geochimica et Cosmochimica Acta*, **64**, 3871 (2000).

D. J. Cherniak and E. B. Watson, Diffusion in zircon. In: J. M. Hanchar and J. M. Hoskin (Eds.), Zircon, *Reviews in Mineralogy and Geochemistry*, **53**, 113 (2003).

D. J. Cherniak, E. B. Watson, M. Grove and T. M. Harrison, Pb diffusion in monazite: A combined RBS/SIMS study, *Geochimica et Cosmochimica Acta*, **68**, 829 (2004).

D. J. Cherniak and E. B. Watson, Ti diffusion in zircon, *Chemical Geology*, **242**, 470 (2007).

D. J. Cherniak and J. M. Pyle, Th diffusion in monazite, *Chemical Geology*, **256**, 52 (2008).

D. Chew and R. Spikings, Geochronology and thermochronology using apatite: U-Pb, Lu-Hf, fission track and (U-Th)/He, *Elements*, **11**, 179 (2015).

A. Cocherie, E. Be Mezeme, O. Legendre, C. M. Fanning, M. Faure and P. Rossi, Electron-microprobe dating as a tool for determining the closure of Th-U-Pb systems in migmatitic monazites, *American Mineralogist*, **90**, 607 (2005).

D. Davis, I. S. Williams and T. Krogh, Historical development of zircon geochronology. In: J. M. Hanchar and J. M. Hoskin (Eds.), Zircon, *Reviews in Mineralogy and Geochemistry*, **53**, 145 (2003).

G. Dumond, N. McLean, M. L. Williams, M. J. Jercinovic and S. A. Bowring, High-resolution dating of granite petrogenesis and deformation in a lower crustal shear zone: Athabasca granulite terrane, western Canadian Shield, *Chemical Geology*, **254**, 175 (2008).

E. D. A. Ferriss, E. J. Essene and U. Becker, Computational study of the effect of pressure on the Ti-in-zircon geothermometer, *European Journal of Mineralogy*, **20**, 745 (2008).

J. M. Ferry and E. B. Watson, New thermodynamic models and revised calibrations for the Ti-in-zircon and Zr-in-rutile thermometers, *Contributions to Mineralogy and Petrology*, **154**, 429 (2007).

F. Finger, I. Broska, M. P. Robers and A. S. Schermailer, Replacement of primary monazite by apatite-allanite-epidote coronas in an amphibolite-facies granite gneiss from the eastern Alps, *American Mineralogist*, **83**, 248 (1998).

F. Finger and E. Krenn, Three metamorphic monazite generations in a high-pressure rock from the Bohemian Massif and the potentially important role of apatite in stimulating polyphase monazite growth along a PT loop, *Lithos.*, **95**, 103 (2007).

H. -J. Förster, The chemical composition of REE-Y-Th-U-rich accessory minerals from peraluminous granites of the Erzgebirge-Fichtelgebirge region, Germany. Part I: The monazite-(Ce)—brabantite solid solution series, *American Mineralogist*, **83**, 259 (1998).

H. -J. Förster and D. E. Harlov, Monazite-(Ce)—huttonite solid solutions in granulite-facies metabasites from the Ivrea-Verbano Zone, Italy, *Mineralogical Magazine*, **63**, 587 (1999).

G. Franz, G. Andrehs and D. Rhede, Crystal chemistry of monazite and xenotime from Saxothuringian-Moldanubian metapelites, NE Bavaria, Germany, *European Journal of Mineralogy*, **8**, 1097 (1996).

T. Geisler, U. Schaltegger and F. Tomaschek, Re-equilibration of zircon in aqueous fluids and melts, *Elements*, **3**, 43 (2007).

R. Gieré, C. T. Williams and G. R. Lumpkin, Chemical characteristics of natural zirconolite, *Schweizerische Mineralogische und Petrographische Mitteilungen*, **78**, 433 (1998).

P. Goncalves, M. L. Williams and M. J. Jercinovic, Electron-microprobe age mapping of monazites, *American Mineralogist*, **90**, 578 (2005).

R. Gratz and W. Heinrich, Monazite-xenotime thermobarometry: Experimental calibration of the miscibility gap in the binary system $CePO_4$-YPO_4, *American Mineralogist*, **82**, 772 (1997).

R. Gratz and W. Heinrich, Monazite-xenotime thermometry. III. Experimental calibration of the partitioning of gadolinium between monazite and xenotime, *European Journal of Mineralogy*, **10**, 579 (1998).

E. C. Hansen and D. E. Harlov, Phosphate, silicate and fluid composition across an amphibolite- to granulite-facies transition, Tamil Nadu, India, *Journal of Petrology*, **48**, 1641 (2007).

S. L. Harley and N. M. Kelly, The impact of zircon-garnet REE distribution data on the interpretation of zircon U/Pb ages in complex high-grade terrains: An example from the Rauer Islands, East Antarctica, *Chemical Geology*, **241**, 62 (2007).

D. E. Harlov and H. J. Förster, High-grade fluid metasomatism on both local and a regional scale: The Seward peninsula, Alaska, and the Val Strona di Omegna, Ivrea-Verbano zone, northern Italy. Part II: Phosphate mineral chemistry, *Journal of Petrology*, **43**, 801 (2002).

D. E. Harlov, U. B. Andersson, H. -J. Förster, J. O. Nyström, P. Dulski and C. Broman, Apatite-monazite relations in the Kiirunavaara magnetite-apatite ore, northern Sweden, *Chemical Geology*, **191**, 47 (2002a).

D. E. Harlov, H. -J. Förster and T. G. Nijland, Fluid-induced nucleation of REE-phosphate minerals in apatite: Nature and experiment, Part I. Chlorapatite, *American Mineralogist*, **87**, 245 (2002b).

D. E. Harlov and H. -J. Förster, Fluid-induced nucleation of (Y+REE)-phosphate minerals within apatite: Nature and experiment, Part II. Fluorapatite, *American Mineralogist*, **88**, 1209 (2003).

D. E. Harlov, R. Wirth and H. -J. Förster, An experimental study of dissolution-reprecipitation in fluorapatite: Fluid infiltration and the formation of monazite, *Contributions to Mineralogy and Petrology*, **150**, 268 (2005).

D. E. Harlov, P. Tropper, W. Seifert, T. Nijland and H.-J. Förster, Formation of Al-rich titanite ($CaTiSiO_4O$–$CaAlSiO_4OH$) reaction rims on ilmenite in metamorphic rocks as a function of fH_2O and fO_2, *Lithos*., **88**, 72 (2006).

D. E. Harlov, H. Marshall and R. Hanel, Fluorapatite-monazite relationships in granulite-facies metapelites, Schwarzwald, Southwest Germany, *Mineralogical Magazine*, **71**, 143 (2007a).

D. E. Harlov, R. Wirth and C. J. Hetherington, The relative stability of monazite and huttonite at 300–900°C and 200–1000 MPa: Metasomatism and the propagation of metastable mineral phases, *American Mineralogist*, **92**, 1652 (2007b).

D. E. Harlov, V. Prochazka, H. -J. Förster and M. Dobroslav, Origin of monazite-xenotime-zircon-fluorapatite assemblages in the peraluminous Melechov granite massif, Czech Republic, *Mineralogy and Petrology*, **94**, 9 (2008).

D. E. Harlov and C. J. Hetherington, Partial high-grade alteration of monazite using alkali-bearing fluids: Experiment and nature, *American Mineralogist*, **95**, 1105 (2010).

D. E. Harlov and D. J. Dunkley, Experimental high-grade alteration of zircon using alkali- and Ca-bearing solutions: Resetting the zircon geochronometer during metasomatism, Abstract V41D-2301 presented at 2010 Fall Meeting, AGU, San Francisco, Calif., 13–17 December 2010.

D. E. Harlov, Formation of monazite and xenotime inclusions in fluorapatite megacrysts, Gloserheia Granite Pegmatite, Froland, Bamble Sector, southern Norway, *Mineralogy and Petrology*, **102**, 77 (2011).

D. E. Harlov, R. Wirth and C. J. Hetherington, Fluid-mediated partial alteration in monazite: The role of coupled dissolution–reprecipitation in element redistribution and mass transfer, *Contributions to Mineralogy and Petrology*, **162**, 329 (2011).

D. E. Harlov and R. Wirth, Experimental incorporation of Th into xenotime at middle to lower crustal P-T utilizing alkali-bearing fluids, *American Mineralogist*, **97**, 641 (2012).

W. Heinrich, G. Andrehs and G. Franz, Monazite-xenotime miscibility gap thermometry. I. An empirical calibration, *Journal of Metamorphic Geology*, **15**, 3 (1997).

C. J. Hetherington and D. E. Harlov, Metasomatic thorite and uraninite inclusions in xenotime and monazite from granitic pegmatites; Hidra anorthosite massif, southwestern Norway: Mechanics and fluid chemistry, *American Mineralogist*, **93**, 806 (2008).

C. J. Hetherington, M. J. Jercinovic, M. L. Williams and K. Mahan, Understanding geologic processes with xenotime: Composition, chronology, and a protocol for electron probe microanalysis, *Chemical Geology*, **254**, 133 (2008).

C. J. Hetherington, D. E. Harlov and B. Budzyn, Experimental metasomatism of monazite and xenotime: Mineral stability, REE mobility and fluid composition, *Mineralogy and Petrology*, **99**, 165 (2010).

J. Hiess, A. P. Nutman, V. C. Bennett and P. Holden, Ti-in-zircon thermometry applied to contrasting Archean metamorphic and igneous systems, *Chemical Geology*, **247**, 323 (2008).

P. W. O. Hoskin and U. Schaltegger, The composition of zircon and igneous and metamorphic petrogenesis. In: J. M. Hanchar and P. W. O. Hoskin (Eds.), Zircon, *Reviews in Mineralogy and Geochemistry*, **53**, 27 (2003).

E. Janots, M. Engi, D. Rubatto, A. Berger, C. Gregory and M. Rahn, Metamorphicrates in collisional orogeny from in situ allanite and monazite dating, *Geology*, **37**, 11 (2009).

T. Kebede, K. Horie, H. Hidaka and K. Terada, Zircon microvein in peralkaline granitic gneiss, Western Ethiopia: origin, SHRIMP U/Pb geochronology and trace element investigations, *Chemical Geology*, **242**, 76 (2007).

M. Kohn, Models of garnet differential geochronology, *Geochimica et Cosmochimica Acta*, **73**, 170 (2009).

N. Kositcin, N. J. McNaughton, B. J. Griffin, I. R. Fletcher, D. I. Groves and B. Rasmussen, Textural and geochemical discrimination between xenotime of different origin in the Archaean Witwatersrand Basin, South Africa, *Geochimica et Cosmochimica Acta*, **67**, 709 (2003).

E. Krenn, K. Ustaszewski and F. Finger, Detrital and newly formed metamorphic monazite in amphibolite-facies metapelites from the Motajica Massif, Bosnia, *Chemical Geology*, **254**, 164 (2008).

K. H. Mahan, M. L. Williams, R. M. Flowers, M. J. Jercinovic, J. A. Baldwin and S. A. Bowring, Geochronological constraints on the Legs Lake shear zone with implications for regional exhumation of lower continental crust, western Churchill Province, Canadian Shield, *Contributions to Mineralogy and Petrology*, **152**, 223 (2006a).

K. H. Mahan, P. Goncalves, M. L. Williams and M. J. Jercinovic, Dating metamorphic reactions and fluid flow: Application to exhumation of high-P granulites in a crustal-scale shear zone, western Canadian Shield, *Journal of Metamorphic Geology*, **24**, 193 (2006b).

Y. Pan, M. E. Fleet and N. D. Macrae, Oriented monazite inclusions in apatite porphyroblasts from the Hemlo gold deposit, Ontario, Canada, *Mineralogical Magazine*, **57**, 697 (1993).

Y. Pan and M. E. Fleet, Composition of the apatite-group minerals: Substitution mechanisms and controlling factors. In: M. J. Kohn, J. Rakovan and J. M. Hughes (Eds.), Phosphates: Geochemical, Geobiological and Materials Importance, Reviews in Mineralogy, *Mineralogical Society of America*, *Washington*, *D.C.,* **48**, 13 (2002).

F. Poitrasson, S. Chenery and D. J. Bland, Contrasted monazite hydrothermal alteration mechanisms and their geochemical implications, *Earth and Planetary Science Letters*, **145**, 79 (1996).

A. Putnis, Mineral replacement reactions: From macroscopic observations to microscopic Mechanisms, *Mineralogical Magazine*, **66**, 689 (2002).

A. Putnis, Mineral replacement reactions. Thermodynamics and kinetics of water-rock interaction. In: E. H. Oelkers and J. Schott (Eds.), *Reviews in Mineralogy and Geochemistry*, **70**, 87 (2009).

J. M. Pyle and F. S. Spear, An empirical garnet (YAG)—Xenotime thermometer, *Contributions to Mineralogy and Petrology*, **138**, 51 (2000).

J. M. Pyle, F. S. Spear, R. L. Rudnick and W. F. McDonough, Monazite-xenotime-garnet equilibrium in metapelites and a new monazite-garnet thermometer, *Journal of Petrology*, **42**, 2083 (2001).

J. M. Pyle and F. S. Spear, Four generations of accessory phase growth in low-pressure migmatites from SW New Hampshire, USA, *American Mineralogist*, **88**, 338 (2003).

J. M. Pyle, F. S. Spear, D. A. Wark, C. G. Daniel and L. C. Storm, Contributions to precision and accuracy of monazite microprobe ages, *American Mineralogist*, **90**, 547 (2005).

D. Rubatto, O. Muentener, A. Barnhoorn and C. Gregory, Dissolution-reprecipitation of zircon at low-temperature, high-pressure conditions (Lanzo Massif, Italy), *American Mineralogist*, **93**, 1519 (2009).

B. Schulz, R. Klemd and H. Braetz, Host rock compositional controls on zircon trace element signatures in metabasites from the Austroalpine basement, *Geochimica et Cosmochimica Acta*, **70**, 697 (2006).

A. M. Seydoux-Guillaume, J. L. Paquette, M. Wiedenbeck, J. M. Montel and W. Heinrich, Experimental resetting of the U-Th-Pb systems in monazite, *Chemical Geology*, **191**, 165 (2002a).

A. M. Seydoux-Guillaume, R. Wirth, W. Heinrich and J. M. Montel, Experimental determination of Thorium partitioning between monazite and xenotime using analytical electron microscopy and X-ray diffraction Rietveld analysis, *European Journal of Mineralogy*, **14**, 869 (2002b).

A. M. Seydoux-Guillaume, P. Goncalves, R. Wirth and A. Deutsch, Transmission electron microscope study of polyphase and discordant monazites: Site-specific specimen preparation using the focused ion beam technique, *Geology*, **31**, 973 (2003).

F. S. Spear, Monazite–allanite phase relations in metapelites, *Chemical Geology*, **279**, 55 (2010).

M. R. St Onge, N. Wodicka and O. Ijewliw, Polymetamorphic evolution of the Trans-Hudson orogen, Baffin Island, Canada: Integration of petrological, structural, and geochronological data, *Journal of Petrology*, **48**, 271 (2007).

M. Thöni, Ch. Miller, A. Zanetti, G. Habler and W. Goessler, Sm–Nd isotope systematics of high-REE accessory minerals and major phases: ID-TIMS, LA-ICP-MS and EPMA data constrain multiple Permian–Triassic pegmatite emplacement in the Koralpe, Eastern Alps, *Chemical Geology*, **254**, 216 (2008).

E. B. Watson, D. A. Wark and J. B. Thomas, Crystallization thermometers for zircon and rutile, *Contributions to Mineralogy and Petrology*, **151**, 413 (2006).

M. L. Williams, M. J. Jercinovic, P. Gonclaves and K. Mahan, Format and philosophy for collecting, compiling, and reporting microprobe ages, *Chemical Geology*, **225,** 1 (2006).

M. L. Williams, M. J. Jercinovic and C. J. Hetherington, Microprobe monazite geochronology: Understanding geologic processes by integrating composition and chronology, *Annual Review of Earth and Planetary Sciences*, **35**, 137 (2007).

M. L. Williams, M. J. Jercinovic, D. E. Harlov, B. Budzy and C. J. Hetherington, Resetting monazite ages during fluid-related alteration, *Chemical Geology*, **283**, 218 (2011).

B. Wing, J. M. Ferry and T. M. Harrison, Prograde destruction and formation of monazite and allanite during contact and regional metamorphism of pelites: Petrology and geochronology, *Contributions to Mineralogy and Petrology*, **145**, 228 (2003).

M. B. Wolf and D. London, Incongruent dissolution of REE- and Sr-rich apatite in peraluminous granitic liquids: Differential apatite, monazite, and xenotime solubilities during anatexis, *American Mineralogist*, **80**, 765 (1995).

Y. Wu, Y. Zheng, S. Gao, W. Jiao and Y. Liu, Zircon U-Pb age and trace element evidence for Paleoproterozoic granulite-facies metamorphism and Archean crustal rocks in the Dabie Orogen, *Lithos.*, **101**, 308 (2008).

X. K. Zhu and R. K. O'Nion, Zonation of monazite in metamorphic rocks and its implications for high temperature thermochronology: A case study from the Lewisian terrain, *Earth and Planetary Science Letters*, **171**, 209 (1999).

M. A. Ziemann, H. -J. Förster, D. E. Harlov and D. Frei, Origin of fluorapatite–monazite assemblages in a metamorphosed, sillimanite- bearing pegmatoid, Reinbolt Hills, East Antarctica, *European Journal of Mineralogy*, **17**, 567 (2005).

Daniel E. Harlov is a research scientist at the Deutsches GeoForschungsZentrum, Potsdam, Germany and a visiting Professor in the Department of Geology, University of Johannesburg. He has degrees from the University of Wisconsin-Madison and Purdue University. His research philosophy is to couple field observation with experimental replication and thermodynamic verification. Current field projects are worldwide and focus on the role of fluids during a wide variety of geological processes. Current laboratory projects focus on mineral-mineral and mineral-fluid equilibria and mineral alteration (apatite, monazite, xenotime, allanite, zircon, titanite, garnet, feldspars, scapolite, oxides, sulphides) under a broad range of P-T-X conditions.